

MODELING AND EXPERIMENT OF SLAG CORROSION ON THE LIGHTWEIGHT ALUMINA REFRACTORY WITH STATIC MAGNETIC FIELD FACING GREEN METALLURGY

A. Huang^{a,b,*}, P. Lian^a, L. Fu^a, H. Gu^a, Y. Zou^a

^a The State Key Laboratory of Refractories and Metallurgy, Wuhan University of Science and Technology, Wuhan, China

^b School of Metallurgy, Northeastern University, Shenyang, Liaoning, China

(Received 14 October 2017; accepted 19 March 2018)

Abstract

Electromagnetic field is applied widely in metallurgy and other high temperature processes, and affects the behavior of melts. The lightweight alumina based carbon free refractory is of importance for energy-saving, consumption reduction and high quality steel production, and the slag corrosion resistance is significant concerning its service life. Does electromagnetic field control the slag corrosion behavior on the lightweight alumina refractory? In this paper, a multi-field coupled model was established to describe the slag corrosion process in an electromagnetic field. The mathematical modeling in combination of experiments was applied to clarify slag corrosion behavior of lightweight alumina refractory in static magnetic field. The simulation results agree with that of the experiments, which means the proposed model is promising for slag corrosion modeling. The results show that the combination of the slag properties change, and electromagnetic damping caused by MHD (magnetohydrodynamics) effect can enhance the slag corrosion resistance by inhibiting slag penetration and promoting formation of a directional isolation layer, and be beneficial to high-quality clean steel production.

Keywords: Electromagnetic field; Lightweight alumina; Slag corrosion; Mathematical modeling; Green metallurgy

1. Introduction

Electromagnetic field is widely discovered and applied in metallurgy and other high temperature processes, and its thermal and mechanical effects are important means of producing special steels and improving the quality of steel [1,2]. Refractory is an essential material to ensure the production, operation, and technological development of high temperature industries. It is involved in the high temperature melting process of ironmaking and steelmaking, and is also the main source of impurities in steel [3,4]. Lightweight refractory is a significant development direction of refractory materials, of which the investigation of slag corrosion behavior and its control mechanism under electromagnetic field has theoretical and practical significance for high quality steels and reducing consumption.

Although flake graphite can protect refractory from being wetted by molten slag, carbon containing refractory has higher heat conductivity and risk of carbon pickup. Therefore alumina based carbon-free refractory is widely used as wear lining in the high temperature industry like ironmaking and steelmaking. In contact with melts, they suffer

corrosion and degradation by slag penetration and dissolution into molten slag. With the extensive studies of corrosion mechanism and slag resistance of in-service refractories, some progresses have been achieved [5-7]. Firstly the molten slag penetrates into the refractories through the pores [8], then the important mechanism which influences the wear rate of refractories is dissolution, whereby a solid, such as a refractory oxide, dissolves in molten slag [9-12]. Normally, the refractory oxides dissolution into molten slags is governed by diffusion due to rapid chemical reactions [12]. Sarpoolaky and Zhang [6,11] studied slag corrosion of different alumina materials and found that a continuous CA_6 ($CaO \cdot 6Al_2O_3$) layer may be formed on the interface of alumina and slag, which leads to the dissolution of alumina into indirect dissolution. Fu and Huang [13,14] investigated slag corrosion behavior of lightweight alumina refractories, and pointed out that the expected phase is more easily supersaturated, precipitation and ripening at a high rate with the decrease of the micro-pore size of alumina aggregates; the critical pore diameter for forming a continuous CA_6 and CA_2 ($CaO \cdot 2Al_2O_3$) isolation layer is $0.5\mu m$ in contact with corresponding $CaO-SiO_2-Al_2O_3$ slag, it can effectively prevent

*Corresponding author: huangao@wust.edu.cn



further corrosion. Meanwhile, due to the rapid renewal of the molten slag in the pores, the lower the viscosity of molten slag is, the smaller the critical pore size is expected as a prerequisite for the formation of continuous isolation [15].

In the condition of electromagnetic field, Li [16,17] carried out experiments and dynamic analysis on slag corrosion of MgO-C refractories by applying induction furnace, and found that the electromagnetic field contributes to high-iron slag penetration on MgO-C refractories due to the penetration of Fe^{2+} in the slag and the carbon containing refractories with a relative high conductivity; Meanwhile the electromagnetic effect will enhance the solution of MgO and power of Mg (g) discharge, so that Mg(g) is uncrystallizable and grows up at the interface, inhibits the formation of MgO compact layer, and then increases corrosion. Okazawa [18] measured the viscosities of molten oxides and mold powders under the isothermal electric field conditions, the results show that when the direct-current (DC) is applied, the viscosity of the molten slag decreases to a certain extent, and the viscosity of the molten slag rises when the alternating-current (AC) is used. In addition, Wang [19] has indicated that the viscosities of mold fluxes increase and the crystal sizes decrease significantly under a high-frequency electromagnetic field. As regards the wettability, Pötschke [20] has noted that an electric field affects the permeation behavior of molten slag, suggesting that an electric double layer forms between refractories and molten slag in high temperature, which affects the slag wettability on the refractory material. Khoroshavin [21] theoretically discussed the impact of electronic technology on the performance of refractories, and predicted that the electromagnetic field would affect the movement of electrons in the redox reaction. Further, Aneziris [22] performed wettability experiments under an electric field, reporting that the electric field can change the wettability between slag and magnesia, promote electron transfer and interfacial reaction, affect the generation and distribution of the high-temperature phases, and accelerate magnesia dissolution in the slag.

Thereby, it is challenging to investigate the slag corrosion process just by available experimental methods, which is not only related to the slag properties and temperature, but also affected by the microstructure of refractories, especially the lightweight materials with much more pores. Berjonneau [23] performed thermodynamic simulations at a constant temperature and pressure to understand the corrosion mechanism by using Factsage software. Luz [24] applied experimental tests and improved the thermodynamic simulation by considering the compositions change of the reacted slag. Harmuth [25] applied CFD (Computational

Fluid Dynamics) simulations to investigate the refractories wear by dissolution. Due to the obvious influence of microstructure parameters such as pore size and porosity [26], Huang [13,27] proposed a model including the description of the microstructure difference, and investigated slag penetration into the lightweight refractories with different aggregates by mathematical simulations.

To summarize the above reports, it has been shown that an electromagnetic field has a significant influence on the properties of slag and on the slag/refractory interaction under high temperature. However, as current research has focused on the influence of the electric field, the independent action of the magnetic field remains unknown. In this work, a micro-CFD (Computational Fluid Dynamics), temperature, reaction and electromagnetic-effect coupled model was established to describe the slag corrosion process in an electromagnetic field. The mathematical modeling in combination of experiments was applied to clarify slag corrosion behavior of lightweight alumina refractory in static magnetic field.

2. Experimental

Lightweight alumina castables were prepared with 70wt% lightweight alumina particles of 0.088~8 mm in diameter and 30wt% alumina powder (<0.088 mm) as raw materials (Jiangsu Jingxin New Material Co., Ltd., China). The apparent porosity and bulk density of the samples were measured according to ISO 5017:1998. The true density and median pore diameter were measured by an automatic true density analyzer (ACCUPYC 1330, Micromeritics Instrument Corporation, Norcross, USA) and mercury intrusion porosimetry measurement (AutoPore IV 9500, Micromeritics Instrument Corporation, Norcross, USA). Physical properties of the lightweight alumina aggregates are listed in Table 1.

Table 1. Physical properties of the lightweight alumina aggregates and matrix

	Bulk density /g·cm ⁻³	True density /g·cm ⁻³	Apparent porosity /%	Median pore diameter/ μ m
Aggregate	3.36	3.92	5	~0.5
Matrix	2.62	3.92	20	~4

The analytical reagent powders, of which 60wt% CaO (Tianjin Bodi Chemical Co., Ltd., China), 20wt% Al₂O₃ (Sinopharm Chemical Reagent Co., Ltd., China), and 20wt% SiO₂ (Tianjin Bodi Chemical Co., Ltd., China) were mixed with a planetary ball mill (QM-BP, Nanjing Nanda Instrument Plant, China) for 30 mins, were pre-melted at 1600 °C for 3 h and



quenched to synthesize the lime-alumina-silica slag. Then the solidified slag was milled to powders with particle size smaller than 0.088 mm. The experiments were performed according to Figure 1. Electromagnetic coil with an adjustable DC stabilized voltage supply was selected to obtain a static magnetic field inside the furnace. Subsequently, the slag powder was pressed to $\Phi 3 \times 3$ mm² cylindrical specimens, which located on an alumina substrate in the center of the furnace and soaked in 1600 °C for 3 mins, and the wettability of the slag was measured through the quenched spread samples [28]. Moreover, the 200g slag was added to alumina crucibles, which were heated at 5 °C/min and soaked in 1600 °C in a static magnetic field, rotating cylinder method and dipping cylinder method (DV2T Brookfield) were applied to measure apparent viscosity and surface tension. In order to ensure the reliability of the experimental results, two samples of each type were tested. The lightweight alumina crucibles of $\Phi 50 \times 50$ mm² (the aperture is $\Phi 37 \times 60$ mm² with 6 g slag) were applied to carry out slag corrosion test by adopting the static crucible method. The crucibles were heated at a temperature of 1600°C for 30 minutes, under the condition of a static magnetic field or without magnetic field, and subsequently quenched. The microstructures of the samples with alumina/slag interface were examined using scanning electron microscopy (SEM, JSM-6610, Jeol, Tokyo, Japan) and the X-ray energy dispersive spectroscopy (EDX, Quantax, Bruker, Berlin, Germany) was used for composition identification.

3. Mathematical model

3.1. Geometric and penetration model

The geometric model of the lightweight castable in contact with molten slag is same as that in the literature [27], in which the aggregates and matrix were separately expressed with different parameters as porous media according to Ergun equations could be added to momentum equation as source term [13]. The developed Ergun equation is expressed as:

$$\frac{\Delta P}{L} = A_1 \frac{\mu v (1-\varepsilon)^2}{d_p^2 \varepsilon^3} + A_2 \frac{\rho v^2 (1-\varepsilon)}{d_p \varepsilon^3} \quad (1)$$

Where ΔP is the pressure drop, Pa; L is the penetration distance in one direction, m; v is the superficial velocity, m/s; ε is the porosity of the porous medium, %; μ is the dynamic viscosity, Pa·s; ρ is the density of fluid, kg/m³; A_1 and A_2 are empirical constants.

The Volume of Fluid (VOF) model was applied to describe a two phase flow comprising liquid and gas (e.g. slag and air), and the flow resistance coefficient equations (2) and (3) are as follows.

$$\frac{1}{a} = 0.2116 \frac{A_1 (1-\varepsilon)^2}{d^2 \varepsilon^2} \quad (2)$$

$$C_2 = 0.92 \frac{A_2 (1-\varepsilon)}{d \varepsilon^{2.5}} \quad (3)$$

Where $1/a$ and C_2 are the viscous resistance coefficient and inertial resistance coefficient, respectively; d is the pore diameter, m; ε is the

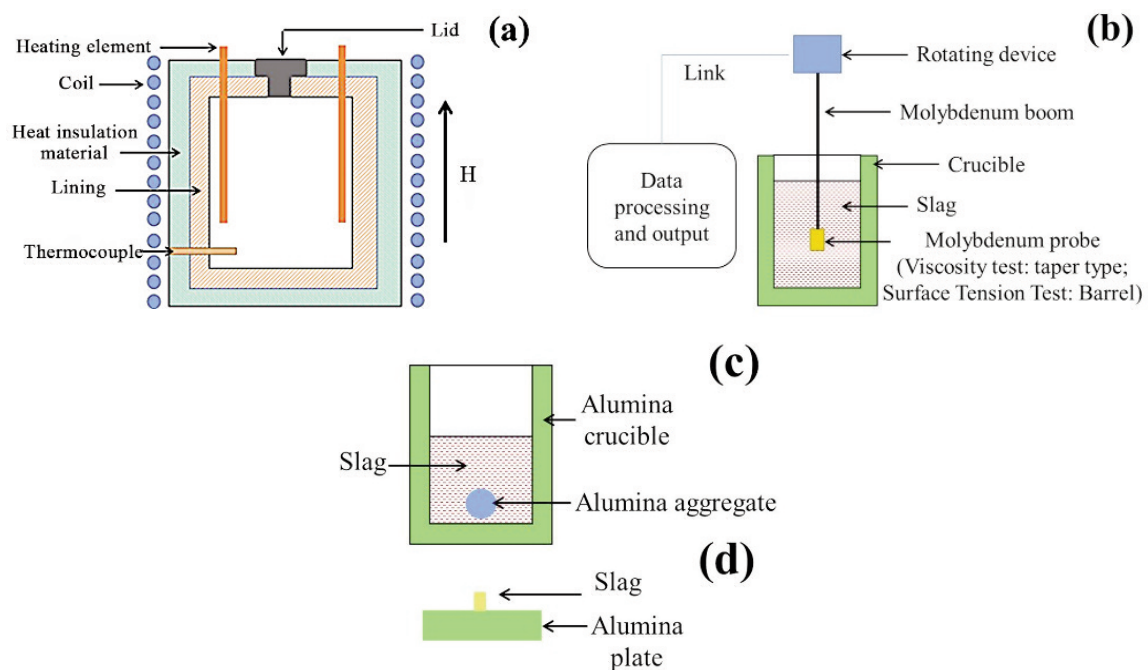


Figure 1. Schematic of experimental apparatus: (a) Schematic of furnace, (b) Apparent viscosity and surface tension test, (c) Corrosion of alumina aggregate, and (d) Wetting behavior of slag on alumina plate

porosity of porous medium, %, A_1 and A_2 are empirical constants which were determined by permeability test [29], for the aggregates, $A_{1,ag}$ is 1216.25 and $A_{2,ag}$ is 37945.24; for the matrix, $A_{1,ma}$ is 412.88 and $A_{2,ma}$ is 34707.80.

3.2. Reaction model

In this study, Al_2O_3 was considered as a sole component dissolved in the molten slag governed by diffusion due to the rapid chemical reaction, and the composition of the molten slag will change during the dissolution process. The dissolution rate ($m \cdot s^{-1}$) was calculated under the assumption of a linear interfacial diffusion according to the Nernst equation [12]:

$$V_{so} = \frac{\rho_{sl}}{100\rho_r} \beta (C_s - C_0) \quad (4)$$

Where ρ_{sl} is the density of the molten slag, $kg \cdot m^{-3}$; ρ_r is the true density of the alumina refractory, $kg \cdot m^{-3}$; C_s is the saturation concentration of the Al_2O_3 in the interface of the flowing slag, wt%; C_0 is the initial concentration of the Al_2O_3 in the slag, which would increase due to dissolution of the Al_2O_3 , wt%; β is the mean mass transfer coefficient, $m \cdot s^{-1}$, which is obtained from the literature [15]; According to the Gibbs-Thomson equation, the alumina fines will be still dissolved at the interface and transferred to the slag until Al_2O_3 precipitation in the slag, which will result in supersaturation of molten slag and reaction products precipitation [14]. Thus, C_s could be simulated by thermodynamic software named FactSage [30], and the reaction products predicted based on the minimization of the free energy of the system, in order to find out the chemical and phase composition at the thermodynamic equilibrium by using the Equilib module [24]. C_0 is the concentration of alumina in the molten slag in each pore (wt%). With the dissolution of alumina in the molten slag, the value of C_0 increases and can be calculated according to the literatures [15,31].

3.3. Electromagnetic model

The governing equations of electromagnetic field contain several equations, and the induced current density (J) can be calculated by:

$$J = \kappa(-\nabla\phi + u \times B) \quad (5)$$

$$E = -\nabla\phi \quad (6)$$

$$\nabla \cdot J = 0 \quad (7)$$

According to (5) and (7), the potential equation can be obtained:

$$\nabla^2\phi = \nabla \cdot (u \times B) \quad (8)$$

The equation of Electromagnetic force F , which could be added to momentum equation as source term:

$$F = J \times B \quad (9)$$

Where, J is the induced current density, $A \cdot m^{-2}$; κ is the conductivity of the molten slag, $S \cdot m^{-1}$; ϕ is the electric potential, V; u is the flow velocity of molten slag, $m \cdot s^{-1}$; B is the magnetic flux density, T; E is the electric field strength, $V \cdot m^{-1}$; F is the electromagnetic force, N/m^3 .

3.4. Numerical conditions and considerations

It was configured as a slag inlet with a constant pressure condition at the interface of molten slag and lightweight alumina refractory, and the other side was as open boundary condition with a constant atmospheric pressure. A slipping condition was modeled at upper and lower walls by means of symmetry function. The simulations were based on the basic assumptions [13,27] and supplements below:

a) The viscosity and density of the slag were assumed to be constants in each case. b) The pores have spherical shape which was applied to calculate the interface area for dissolution. c) The conglomeration and growth of the new phases occur instantly so that it was ignored, so the slag penetration will not stop until the new phase starts. d) The molten slag does not influence the distribution of magnetic field. e) The conductivity of the slag was assumed to be a constant.

3.5. Computational parameters and simulation

The above modeling concepts have been incorporated into a commercial CFD code. Thereby, the computational domain has been discretized by approximately 1000k mostly quadrilateral cells. A series of simulations were carried out with the parameters in Table 2.

4. Results and discussion

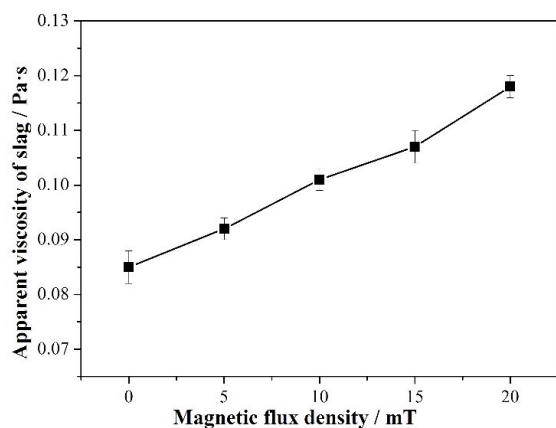
4.1. Slag properties

Slag properties significantly affect the corrosion behavior of refractory materials, especially the apparent viscosity, surface tension of the slag, and slag wetting angle. The apparent viscosity, surface tension of the slag, and slag wetting angle in contact with alumina were studied in a static magnetic field. The apparent viscosities of the molten slag under different magnetic flux intensities are shown in Figure 2, the apparent viscosity increased gradually with the increase of the magnetic flux intensity. Viscosity is the physical property when a fluid resists flow through internal friction and can be quantified to have rheological properties against flow deformation, so the retardation of motion of charged microscopic particles is a major cause of viscosity increase. The



Table 2. The main parameters in simulation at 1600°C

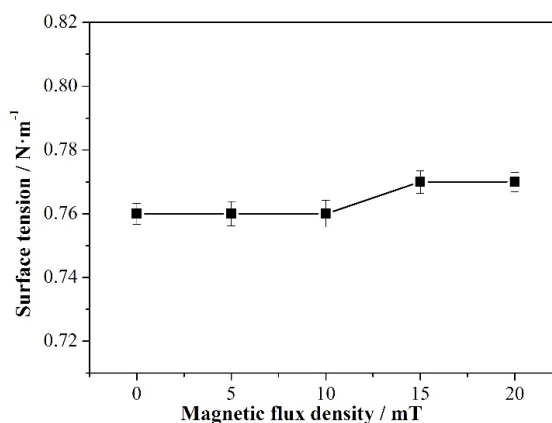
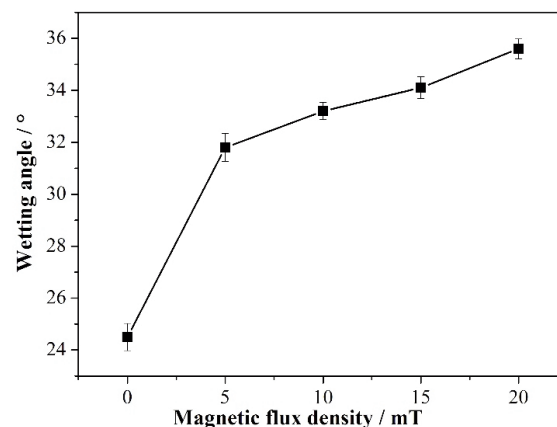
Parameters	Values
Density of slag	2775 /kg·m ⁻³
Wetting angle	24.5 /°
Viscosity of slag	0.085 /Pa·s
Surface tension of slag	0.76 /N·m ⁻¹
Effective diffusion coefficient of Al ₂ O ₃	1.0×10 ⁻¹¹ /m ² ·s ⁻¹
Electrical conductivity of slag	107 /Ω ⁻¹ ·m ⁻¹ [32]

**Figure 2.** Apparent viscosity of the molten slag in a static magnetic field

movement of ions in the molten slag could be slowed down due to the effect of the Lorentz force. As the magnetic flux intensity increased, the Lorentz force increased accordingly, and therefore the value of the apparent viscosity rose linearly. The apparent viscosity of the molten slag was 0.085 Pa·s without a magnetic field. When the magnetic flux intensity reached 20 mT, the apparent viscosity of the slag increased to 0.118 Pa·s.

The surface tensions of the molten slag under different magnetic flux intensities are shown in Figure 3. As the magnetic flux density increased, the surface tension was changed slightly. It indicates that static magnetic field has no obvious effect on the surface tension of the slag, because the surface tension is only related to the stress state of the molecules in the thin layer of the liquid surface.

As shown in Figure 4, when the magnetic flux intensity increased, the wetting angle of the slag in contact with the alumina increased gradually. It indicates that the slag spreading on the alumina substrate was affected by the electromagnetic force which was involved, and changed the balance of three interfacial tensions. When the magnetic flux intensity increased from 0 mT to 5 mT, the wetting angle of the molten slag increased quickly. The growth rate of the slag wetting angle with respect to alumina tended to be constant with increasing of the magnetic flux

**Figure 3.** Surface tension of the molten slag in a static magnetic field**Figure 4.** Wetting angle of slag on the alumina plate in a static magnetic field

intensity more than 5 mT. When the magnetic flux density was 5 mT, the wetting angle of the slag to alumina was 31.8°. While the magnetic flux intensity reached 20 mT, the wetting angle of the slag to alumina increased to 35.6°.

4.2. Slag corrosion

The simulation was stopped at the same reaction time as the experiments, and the calculation of the penetration depth was recorded when the penetration depth ceased to change rapidly. The default value of the pore diameter for aggregates and the matrix was 0.5 μm and 4 μm, respectively, and the temperature was 1600°C. In Figure 5, the red color indicates the area where the slag penetrated through the pores, and the blue area is the original castable with pores.

As shown in Figure 5, the slag infiltrated into the lightweight alumina castable through open pores at a time of 8 s without considering the cracks. It was observed that the porous alumina aggregates with

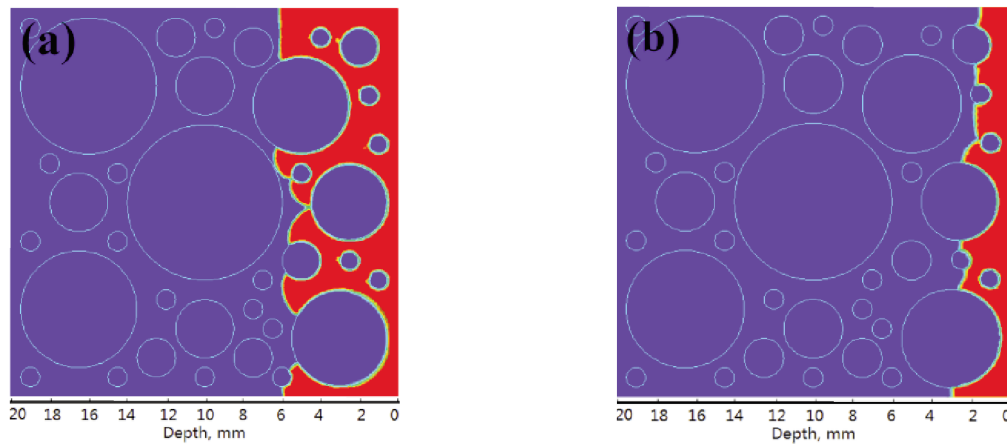


Figure 5. Slag penetration at 8 s (a) without a magnetic field and (b) in a static magnetic field

larger flow resistances blocked the infiltration of the molten slag, so the molten slag move forward in the matrix bypassed these obstructions. Obviously, the slag penetration depth without a magnetic field is almost twice as big as that of the slag penetration depth under a magnetic field. According to the Bilkerman equation [33] below, and the parameters mentioned above, the penetration depth without a magnetic field can be calculated simply:

$$l = \sqrt{r\sigma t \cos\theta / 2\eta} \quad (10)$$

where l is the depth of penetration, t is the time for penetration, η is the dynamic viscosity of molten slag, σ is the surface tension of the slag, r is the pore radius, and θ is the wetting angle.

As shown in Figure 6, the penetration depth of the molten slag increased with time lapse, and the speed of the penetrated molten slag was retarded owing to inertial and viscous resistances. The depth of slag penetration in the simulation is shallower than the calculated value at 8 s, owing to solid precipitation. The slag penetration depth under a constant magnetic field is much shallower than that without a magnetic field at each time. This indicates that the slag penetration was significantly inhibited in a static magnetic field, which is helpful for extending the life of the lining.

The simulated results of the reaction between the molten slag and alumina aggregate are shown in Figure 7. It can be seen that the main product of the slag and alumina was CA_6 , which was formed as a layer. In the absence of a magnetic field, the thickness of the CA_6 layer formed by the reaction of the molten slag with the alumina particles is significantly larger than that of the CA_6 layer under a magnetic field. The thickness of the CA_6 layer is about 64 μm without a magnetic field, while the thickness of the CA_6 layer in a magnetic field is approximately 37 μm . This indicates that the magnetic field may inhibit the diffusion of slag into alumina and the effective penetration of the slag into alumina by the action of an electromagnetic force.

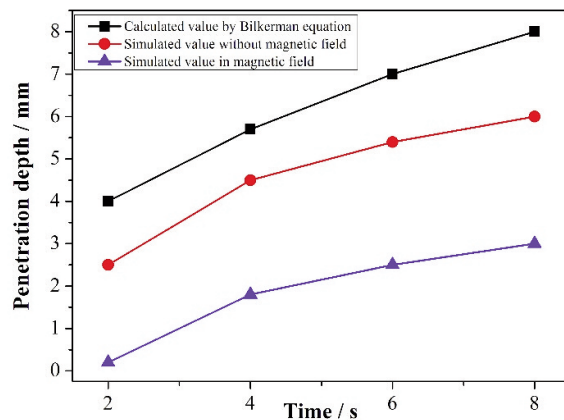


Figure 6. Calculated and simulated slag penetration depth

4.3. Isolation of aggregates

As shown in Figure 8, the CA_6 isolation layer, of which the definition mentioned in the literature [15], is formed at the interface between the corundum particles and the slag under conditions of a magnetic field and no magnetic field. Under the condition of a magnetic field, the thickness of the CA_6 layer formed is approximately 70–90 μm , while the thickness of the larger CA_6 layer formed under a nonmagnetic field is approximately 50–70 μm . In addition, there are many pores in the CA_6 layer under no magnetic field, which indicates that CA_6 is formed during the process of slag corrosion of the alumina aggregate. Under the condition of a magnetic field, a large number of the CA_6 with columnar structure grew towards the slag, of which only approximate 30–40 μm CA_6 layer was in the lightweight refractory (original material) compared to that without a magnetic field shown in Figure 8a). The thickness of the CA_6 layer formed in the refractory without a magnetic field is larger than that of the CA_6 layer under a magnetic field, which is in agreement with the simulation results.

The apparent viscosity of molten slag under the condition of a magnetic field is bigger than that under a

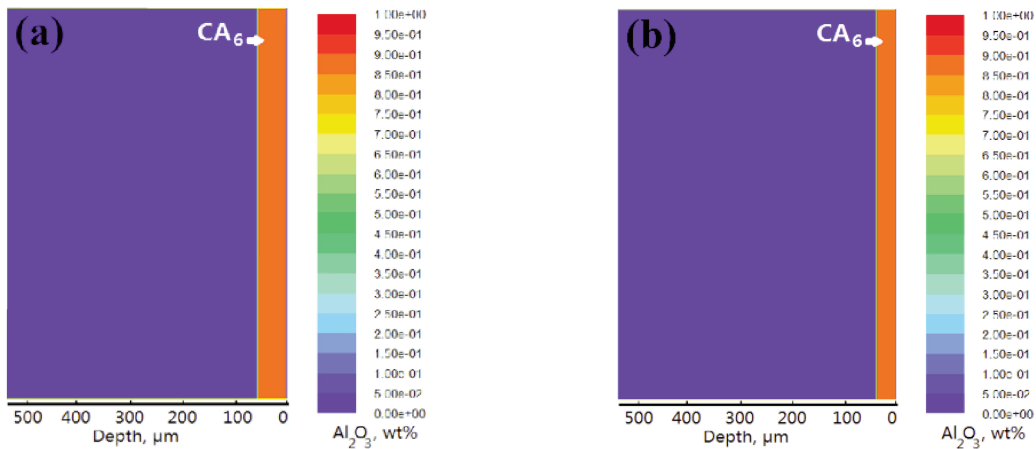


Figure 7. Isolation layer in the aggregates (a) without a magnetic field and (b) in a static magnetic field

nonmagnetic field. In a static magnetic field, the mass transfer between molten slag in the pore and original molten slag slowed down, and the molten slag in the pore would “update” slowly. Hence, molten slag in the pore is easier to be supersaturated with the dissolution of the alumina in a static magnetic field, and the solid phases of calcium aluminates would be precipitated out more easily.

The results discussed above suggest that a magnetic field can not only effectively inhibit the penetration of slag into alumina material, but can also promote the directional growth of CA_6 to form a thicker isolation layer, which is conducive to the protection of lightweight alumina material.

4.4. Effect of magnetic flux density

The effect of magnetic flux density on the slag corrosion of the lightweight alumina material was explored. The slag penetration results are shown in Figure 9, and both simulated and measured depth values are shown in Figure 10. As shown in Figure 9 and 10, as the magnetic flux density increased, the penetration depth of the slag into the lightweight refractory material gradually decreased, mainly in the horizontal direction. On the one hand, the viscosity and wetting angle of the slag were changed with electromagnetic field that was illustrated in Figure 2

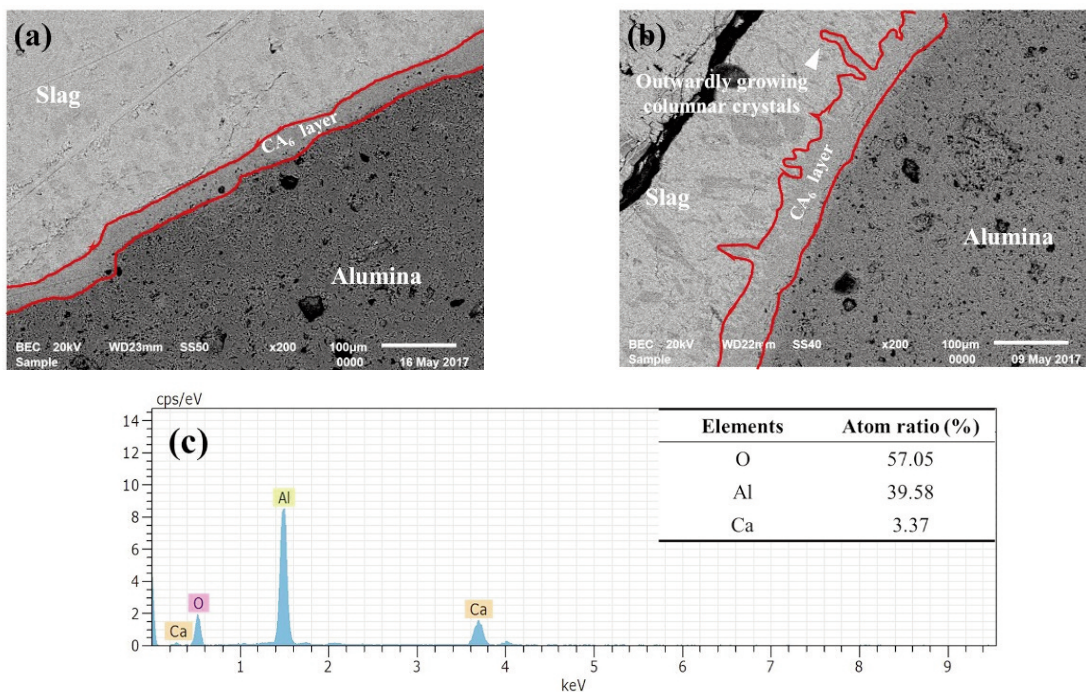


Figure 8. Interfacial microstructure of alumina aggregates and slag after slag corrosion (a) without a magnetic field, (b) in a static magnetic field, and (c) The energy dispersive spectroscopy (EDS) of the isolation layer



and 4. According to the equation (10), the increase of both viscosity and wetting angle of the slag will reduce the depth of slag penetration. On the other hand, molten slag has a certain electrical conductivity, and the electromagnetic force would be formed under a static magnetic field due to the movement of slag cut magnetic lines in the process of slag penetration. When the slag penetrates downwards, the moving direction of the slag is the same as that of the magnetic field, and no electromagnetic force is generated in the slag according to equation (5)~(9). Nevertheless the downward depth of penetration was reduced with the increasing of magnetic flux density especially in 15 mT. It indicates that the combination of slag properties change, and that the electromagnetic damping caused by MHD effect leads to a decrease of depth of the slag penetration under static magnetic field. As shown in Figure 10, although the simulated values are a little smaller than the measured ones due to simplified porous structure parameters, the simulation results agree with that of the experiments in the tendency, which means the proposed model is promising for modeling the process of slag corrosion in a static magnetic field.

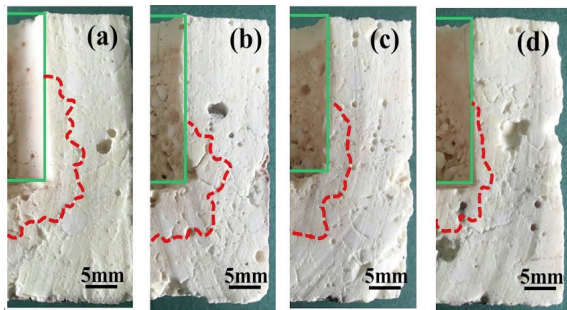


Figure 9 The sectional view of lightweight alumina castable after slag corrosion experiments with different magnetic flux density (a) 0 mT, (b) 5 mT, (c) 10 mT, and (d) 15 mT

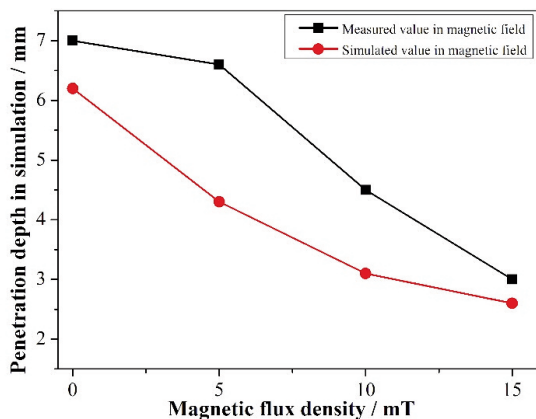


Figure 10. Slag penetration depth in the magnetic field with different magnetic flux density

5. Conclusion

In this study, the apparent viscosity, surface tension of the slag, and slag wetting angle with respect to lightweight alumina were measured in a static magnetic field. A micro-CFD, temperature, reaction, and electromagnetic-effect coupled model was established to describe the slag corrosion process in an electromagnetic field. The mathematical modeling was applied in combination with experiments in order to clarify the slag corrosion behavior of lightweight alumina refractory in a static magnetic field, and the interfacial behavior between the slag and the alumina in a magnetic field was analyzed and discussed.

With an increase in the magnetic flux intensity, the apparent viscosity of the molten slag and the wetting angle of the slag on the alumina gradually increased, while the surface tension of the molten slag did not show an obvious change. The simulation results agree with those of the experiments. This indicates that the proposed model is promising for modeling of slag corrosion in a static magnetic field. In addition, the slag penetration depth under a static magnetic field was much smaller than that without a magnetic field. The combination of slag properties change and electromagnetic damping caused by MHD effect leads to a decrease of depth of the slag penetration under static magnetic field, and inhibits the slag corrosion by promoting the directional growth of CA6 to form a thicker isolation layer. It is conducive to the protection of a lightweight alumina carbon-free material and high quality clean steel production.

Acknowledgement

This work is supported by the National Natural Science Foundation of China (Grant No. 51204126 and U1560208), the International Science & Technology Cooperation Program of Hubei Province of China (Grant No. 2016AHB026), and the Fund for the Excellent Creative Research Groups of Higher Education of Hubei Province of China (Grant No. T201602).

References

- [1] Z. Cao, J. Fei, X. Zhang, H. Hao, J. Jin, *Materials Science & Engineering A*, 327(2) (2002) 133-137.
- [2] Z. Zhang, H. Jia, X. Zhang, K. Deng, Z. Ren, Z. Lei, *Advanced Materials Research*, 402 (2012) 46-50.
- [3] M. C. Mantovani, L. R. Moraes, R. L. D. Silva, E. F. Cabral, E. A. Possente, C. A. Barbosa, B. P. Ramos, *Ironmaking & Steelmaking*, 40(5) (2013) 319-325.
- [4] Z. Deng, M. Zhu, S. Du, *Metallurgical & Materials Transactions B*, 47(5) (2016) 1-10.
- [5] H. Sarpoolaky, S. Zhang, B. B. Argent, W. E. Lee, *Journal of the American Ceramic Society*, 84(2) (2010) 426-434.
- [6] H. Sarpoolaky, S. Zhang, W. E. Lee, *Journal of the*



- European Ceramic Society, 23(2) (2003) 293-300.
- [7] S. Yilmaz, Ironmaking & Steelmaking, 33(2) (2006) 151-156.
- [8] M. Jiang, Z. Chen, Journal of the Chinese Ceramic Society, 18(3) (1990) 256-261.
- [9] Z. Chen, Journal of the Chinese Ceramic Society, 11(4) (1983) 498-507.
- [10] J. L. Bates, Journal of the American Ceramic Society, 70(3) (1987) C-55-C-57.
- [11] S. Zhang, R. H. Reza, S. Hossain, L. W. Edward, Journal of the American Ceramic Society, 83(4) (2000) 897-903.
- [12] J. Pötschke, C. Brüggmann, Steel Research International, 83(7) (2012) 637-644.
- [13] A. Huang, H. Gu, Y. Zou, L. Fu, P. Lian, L. Jin, Ceramic Transactions, 256 (2016) 101-111.
- [14] L. Fu, H. Gu, A. Huang, M. Zhang, Z. Li, Journal of the American Ceramic Society, 98(5) (2015) 1658-1663.
- [15] L. Fu, A. Huang, P. Lian, H. Gu, Corrosion Science, 120C (2017) 211-218.
- [16] X. Li, B. Zhu, T. Wang, Ceramics International, 38(3) (2012) 2105-2109.
- [17] X. Li, B. Zhu, T. Wang, Ceramics International, 38(4) (2012) 2883-2887.
- [18] K. Okazawa, M. Yamane, Y. Fukuda, Tetsu-to-Hagane, 89(6) (2009) 629-636.
- [19] X. Wang, L. Zhu, Y. Zhang, Z. Li, The 2nd National Conference on Electromagnetic Metallurgy and Strong Magnetic Field Materials, 20-23 August, Baotou, China, 2014, p. 21-23.
- [20] J. Pötschke, 51st International Colloquium on Refractories for Metallurgy, 15-16 October, Aachen, Germany, 2008, p. 144-146.
- [21] L. B. Khoroshavin, V. B. Shcherbatskii, Refractories & Industrial Ceramics, 46(5) (2005) 344-351.
- [22] C. G. Aneziris, M. Hampel, International Journal of Applied Ceramic Technology, 5(5) (2008) 469-479.
- [23] J. Berjonneau, P. Prigent, J. Poirier, Ceramics International, 35(2) (2009) 623-635.
- [24] A. P. Luz, A. G. T. Martinez, M. A. L. Braulio, V. C. Pandolfelli, Ceramics International, 37(4) (2011) 1191-1201.
- [25] H. Harmuth, S. Vollmann, Interceram International Ceramic Review, (2) (2011) 88-90.
- [26] K. Mukai, Z. Tao, K. Goto, Z. Li, T. Takashima, Scandinavian Journal of Metallurgy, 31(1) (2010) 68-78.
- [27] A. Huang, H. Gu, Y. Zou, Proceedings of the Unified International Technical Conference on Refractories 2013, 10-13 September, Vancouver, Canada, 2013, p. 863-868.
- [28] J. Choi, H. Lee, Transactions of the Iron & Steel Institute of Japan, 43(9) (2003) 1348-1355.
- [29] Y. Zou, H. Gu, A. Huang, M. Zhang, C. Ji, Ceramics International, 40(5) (2014) 7023-7028.
- [30] C. W. Bale, E. Bélisle, P. Chartrand, S. A. Decterov, G. Eriksson, A. E. Gheribi, et al. Calphad, 54 (2016) 35-53.
- [31] Y. Liang, A. Huang, X. Zhu, H. Gu, L. Fu, Ceramics International, 41(6) (2015) 8149-8154.
- [32] G. Zhang, B. Yan, K. Chou, F. Li, Metallurgical & Materials Transactions B, 42(2) (2011) 261-264.
- [33] N. Li, H. Gu, H. Zhao, Metallurgical Industry Press, Beijing, 2010, p. 50-60.

PRORAČUNAVANJE I EKSPERIMENTISANJE SA KOROZIJOM ŠLJAKE VATROSTALNIH MATERIJALA NA BAZI ALUMINJUMA U STATIČNOM MAGNETNOM POLJU U SKLADU SA ZELENOM METALURGIJOM

A. Huang^{a,b,*}, P. Lian^a, L. Fu^a, H. Gu^a, Y. Zou^a

^a Glavna državna laboratorija za vatrostalnost i metalurgiju, Vuhan Univerzitet za nauku i tehnologiju, Vuhan, Kina

^b Škola metalurgije, Severoistočni Univerzitet, Šenjang, Liaoning, Kina

Apstrakt

Elektromagnetno polje ima široku primenu u metalurškim i ostalim postupcima koji uključuju visoke temperature, i ono utiče na ponašanje istopljenih metala. Vatrostalni materijal na bazi aluminijuma male težine bez ugljenika je veoma važan za štednju energije, smanjenje potrošnje i proizvodnju čelika visokog kvaliteta, kao i za otpornost na koroziju šljake koja znatno utiče na njen upotrební vek. Da li elektromagnetno polje utiče na koroziju šljake dobijene od vatrostalnih materijala na bazi aluminijuma? U ovom radu je korišćen model zasnovan na više polja za opisivanje postupka korozije šljake u elektromagnetnom polju. Korišćen je matematički proračun u kombinaciji sa eksperimentima za objašnjenje ponašanja šljake dobijene od vatrostalnih materijala na bazi aluminijuma prilikom pojave korozije. Rezultati dobijeni prilikom proračuna se slažu sa rezultatima eksperimenta, što dokazuje da je predloženi model pogodan za proračun korozije šljake. Rezultati pokazuju da kombinacija promene osobina šljake i elektromagnetno prigušenje izazvano MHD (magnetnohidronimačkim) efektom može poboljšati otpornost na koroziju kod šljake sprečavanjem prodiranja šljake i formiranjem usmerenog izolacionog sloja, a takođe može biti korisno prilikom čišćenja proizvoda od čistog čelika visokog kvaliteta.

Ključne reči: Elektromagnetno polje; Aluminijum male težine; Korozija šljake; Matematički proračun; Zelena metalurgija

